Strength model for end cover separation failure in RC beams strengthened with near-surface mounted (NSM) FRP strips

Published in:

Document Version:

Queen's University Belfast - Research Portal:

Publisher rights

General rights

Take down policy

Open Access

Strength Model for End Cover Separation Failure in RC Beams Strengthened with Near-surface Mounted (NSM) FRP Strips

J.G. Teng[1,*], S.S. Zhang[2] and J.F. Chen[3]

[1]Department of Civil and Environmental Engineering, The Hong Kong Polytechnic University, Hong Kong, China. Email: cejgteng@polyu.edu.hk

[2]School of Civil, Mining & Environmental Engineering, Faculty of Engineering & Information Sciences, University of Wollongong, Northfields Avenue, Wollongong, NSW 2522, Australia.

[3]School of Planning, Architecture and Civil Engineering, Queen's University Belfast, Belfast BT9 5AG, UK

Abstract: As an alternative to externally bonded FRP reinforcement, near-surface mounted (NSM) FRP reinforcement can be used to effectively improve the flexural performance of RC beams. In such FRP-strengthened RC beams, end cover separation failure is one of the common failure modes. This failure mode involves the detachment of the NSM FRP reinforcement together with the concrete cover along the level of the steel tension reinforcement. This paper presents a new analytical strength model for end cover separation failure in RC beams strengthened in flexure with NSM FRP strips (i.e. rectangular FRP bars with a sectional height-to-thickness ratio not less than 5), which was formulated on the basis of extensive numerical results from a parametric study undertaken using an efficient finite element approach. The proposed strength model consists of an approximate analytical equation for the debonding strain of the FRP reinforcement at the critical cracked section and a conventional section analysis to relate this debonding strain to the moment acting on the same section (i.e. the debonding strain). Once the debonding strain is known, the load level at end cover separation of an FRP-strengthened RC beam can be easily determined for a given load distribution. Predictions from the proposed strength model are compared with those of two existing strength models of the same type and available test results, which shows that the proposed strength model is in close agreement with test results and is far more accurate than the existing strength models.

Keywords: End cover separation, finite element analysis, FRP strengthening, near-surface mounted (NSM) FRP, RC beams, strength model

---

* Corresponding author. Email: cejgteng@polyu.edu.hk; Fax: +852 2766 1354; Tel: +852 2766 6012

1 INTRODUCTION

Extensive research has been undertaken on the flexural strengthening of reinforced concrete (RC) beams using bonded FRP reinforcement. Strengthening using externally bonded FRP reinforcement has received by far the largest amount of research [1-4], but the alternative of near-surface mounted (NSM) FRP reinforcement has also received increasing attention [e.g. 5-8]. The externally bonded FRP method involves the external bonding of FRP laminates, either formed in-situ via the wet layup process or prefabricated off site generally by pultrusion, to the tension surface of RC members, and the NSM FRP method involves the cutting of grooves in the cover concrete and the embedding of FRP bars in the grooves using an adhesive. FRP bars of various cross-sectional shapes can be used in NSM FRP strengthening of structures, including round, square, and rectangular bars [6]. As a special form of rectangular bars with a large cross-sectional height-to-thickness ratio, FRP strips are an attractive form of NSM FRP reinforcement due to their superior bond performance over NSM FRP bars of other shapes. This is because an FRP strip usually has a much larger perimeter for the same cross-sectional area than an FRP bar of other sectional shape and hence better bond performance, allowing a fuller utilization of the tensile strength of the FRP material [e.g. 9, 10]. Against this background, the present study is only concerned with NSM FRP strips which are defined as narrow rectangular FRP bars with a sectional height-to-thickness ratio not less than 5 [11]. For ease of presentation, the discussions in the paper are limited to simply supported beams.

In RC beams strengthened in flexure with NSM FRP bars, several debonding failure modes have been observed in laboratory tests, including end debonding failure and intermediate crack (IC) induced debonding failure. End cover separation (Fig. 1), as one of the end debonding failure modes, has been found to be by far the most common failure mode [6, 8].

2

End cover separation failure process is initiated by the formation of a vertical crack in the un-strengthened region but near the critical end of the FRP reinforcement, followed by the propagation of a major crack at the level of the tension steel reinforcement towards the middle of the strengthened region. Another possible end debonding failure mode, namely interfacial debonding at the FRP-to-concrete interface, has been rarely if ever observed in laboratory tests [8]. A major reason that end cover separation is much more likely than end interfacial debonding is the significant radial stresses generated by the steel tension bars on the surrounding concrete, making the plane of steel tension bars a more critical plane than the plane near the adhesive-concrete bi-material interface [12].

For RC beams strengthened with externally bonded FRP reinforcement, a large number of finite element studies on end cover separation failure have been undertaken [e.g. 13-15] and several analytical strength models for this failure mode have been established [e.g. 16-19]. By contrast, for RC beams strengthened with NSM FRP reinforcement, very limited research has been conducted on finite element modelling [12, 20] or the establishment of strength models [21, 22] for the end cover separation failure mode. This situation is not surprising as the NSM FRP strengthening method emerged much later than the externally bonded FRP method and the associated research challenges are greater due to the presence of a large number of significant parameters.

To predict end cover separation failure in RC beams strengthened with NSM FRP reinforcement, a full 2-D (plane stress) nonlinear finite element (FE) approach (referred to as "the full FE approach" for brevity) has recently been developed by the authors [12, 20]. Using this full FE approach, the important factors that influence the accuracy of FE prediction of end cover separation failure have been identified. One of the factors is the radial

stresses exerted by the steel tension reinforcement onto the surrounding concrete, which was introduced by the authors into FE modelling of end cover separation failure in RC beams strengthened with FRP for the first time [12, 20]. Based on the findings from the full FE approach, a simplified 2-D (plane stress) FE approach (referred to as "the simplified FE approach" for brevity) [23, 24], in which only the part of the RC beam between the two adjacent cracks nearest to the critical end of the FRP reinforcement is included, was established for predicting end cover separation failure. This paper presents a study which was conducted using this simplified FE approach for the development of an analytical debonding strength model for RC beams strengthened with NSM FRP strips.

2   EXISTING STRENGTH MODELS

To date, only two strength models for end cover separation in RC beams strengthened in flexure with NSM FRP have been proposed [21, 22], and both of them are based on the concept of the so-called concrete tooth model (CTM) (Fig. 2). In a CTM, the "tooth" (Fig. 2), which is the concrete cover between two adjacent cracks, is treated as a cantilever, with the horizontal shear stress τ (from the NSM FRP) acting on its tip (i.e. free end). In addition to these two models, Hassan and Rizkalla [25] proposed a model based on interfacial stress analysis between NSM FRP strips and concrete to predict end interfacial debonding failure (another important end failure mode) in RC beams strengthened with NSM CFRP strips. For comparison purposes, Hassan and Rizkalla's model [25] is also introduced in this section although it deals with a slightly different failure mode.

2.1 De Lorenzis and Nanni's model [21]

Based on Zhang et al.'s model (the first CTM for end cover separation) [26] for RC beams strengthened in flexure with an externally bonded steel plate, De Lorenzis and Nanni [21]

4

proposed a strength model for end cover separation in RC beams strengthened in flexure with NSM FRP round bars. Assuming a linear elastic behaviour, the tensile stress σ_A at the tension corner near the root of the concrete tooth (Point A in Fig. 2) can be calculated as

$$\sigma_A = \frac{M_A}{I_A}\left(\frac{l}{2}\right) \tag{1}$$

where $M_A = \tau n \pi d_b l h'$ is the bending moment at the foot of the concrete tooth, $I_A = \frac{bl^3}{12}$ is the sectional moment of area of the concrete tooth cross-section, h' is the vertical distance between the root of the concrete tooth and the centroid of the NSM FRP, b is the width of the RC beam, d_b is the diameter of the FRP round bar, n is the number of the FRP bars, τ is the average interfacial shear stress between the NSM FRP bar and the concrete, and l is either the minimum stabilized crack spacing, l_{min}, or the maximum stabilized crack spacing, $l_{max} = 2l_{min}$. The minimum stabilized crack spacing l_{min} is given by

$$l_{min} = \frac{A_e f_t}{u_s \sum O_{bars} + u_{NSM} \sum O_{NSM}} \tag{2}$$

where $f_t = 0.36\sqrt{f_{cu}}$ (both f_t and f_{cu} are in MPa) is the concrete tensile strength while f_{cu} is the concrete cube compressive strength; $\sum O_{bars}$ is the sum of perimeters of all the steel tension bars; $u_s = 0.28\sqrt{f_{cu}}$ (both u_s and f_{cu} are in MPa) is the average shear bond strength between steel bars and concrete; $\sum O_{NSM}$ is the sum of perimeters of all the NSM FRP round bars; u_{NSM} is the bond strength between NSM FRP bars and concrete; $A_e = 2h_1 b$ is the cross-sectional area of the concrete in the beam that is under tension, which is taken to be the product of twice the distance from the centroid of the tension steel to the soffit of the beam (i.e. h_1) and the beam width. De Lorenzis and Nanni [21] recommended that u_{NSM} be taken as the local bond strength between NSM FRP bars and concrete.

Substituting M_A and I_A into Eq. 1 and assuming that cover separation failure occurs when the tensile stress σ_A is equal to the tensile strength of concrete f_t, the average interfacial shear stress $\tau_{failure}$ at failure can be found as

$$\tau_{failure} = \frac{f_t l}{6h'} \frac{b}{n\pi d_b} \tag{3}$$

The interfacial shear stress is balanced by the axial stress in the FRP. At the critical location (such as the loading point for three-point or four-point bending beams), the critical axial stress in the FRP can be found as

$$\sigma_{failure} = \frac{4\tau_{failure} L_p}{d_b} = \frac{2lbf_t L_P}{3n\pi h' d_b^2} \tag{4}$$

by assuming that the interfacial stress is uniformly distributed over the effective length of the NSM bars L_p. De Lorenzis and Nanni (2003) proposed the following expressions to estimate the effective length L_p:

$$L_p = \min(L_{p1}, L_{p2}) \tag{5}$$

$$L_{p2} = 1.86 l_{min}^2 - 127 l_{min} + 2436 \qquad if \qquad l_{min} \le 50mm \tag{6a}$$

$$L_{p2} = 736 \qquad if \qquad l_{min} > 50mm \tag{6b}$$

where L_{p1} is the length of the NSM FRP bar in the shear span.

2.2 Al-Mahmoud et al.'s model [22]

Al-Mahmoud et al. [22] proposed a strength model of end cover separation in RC beams strengthened with NSM FRP round bars. Their model is also based on the general concept of the CTM, but the methodology is slightly different from that proposed by De Lorenzis and Nanni [21].

Al-Mahmoud et al. [22] related the bending moment at the root of the concrete tooth to the axial stress in the FRP bar at the left cracked section (i.e. the left vertical surface of the concrete tooth in Fig. 2, which is referred to as the critical cracked section in this paper) as

$$M_A = \sigma_f A_f h' = \sigma_f n \pi d_b^2 h' \tag{7}$$

Combining Eqs. 1 and 7 and assuming that end cover separation occurs when the tensile stress σ_A reaches the tensile strength of concrete f_t, the axial stress in the FRP bar at the critical cracked section can be expressed as

$$\sigma_f = \frac{b_c l^2}{6 \pi n d_b^2 h'} f_t \tag{8}$$

The axial stress in the FRP bar can be related to the bending moment M_l of the strengthened beam at the critical cracked section as

$$\sigma_f = n_f \left(\frac{h_0 - y_0}{I_{cr}} \right) M_l \tag{9}$$

where $n_f = E_f / E_c$ is the ratio of elastic modulus between FRP and concrete, I_{cr} is the transformed second moment of area in terms of the concrete of the cracked section, h_0 is the distance between the compression face of the beam and the centroid of the NSM FRP reinforcement, and y_0 is the distance between the top surface of the beam and the neutral axis of the critical cracked section. Combining Eqs. 8 and 9 leads to the following expression for the bending moment of the strengthened beam at the left cracked section at cover separation failure:

$$M_l = \frac{f_t I_{cr} b l^2}{6 n_f n \pi d_b^2 h' (h_0 - y_0)} \tag{10}$$

2.3 Hassan and Rizkalla's model [25]

Hassan and Rizkalla [25] established a model for the end interfacial debonding strength of RC beams strengthened with CFRP strips. Based on the interfacial stress analysis by Malek et al. [27] of RC beams strengthened with an externally bonded FRP plate, Hassan and Rizkalla [25] proposed a closed-form solution for the interfacial shear stress τ between the NSM CFRP strip and the concrete in RC beams strengthened with NSM CFRP strips, which leads to the following two equations for a simply supported beam subjected to 3-point bending (Eq. 11) and 4-point bending (Eq. 12) respectively:

$$\tau = \frac{t_f}{2}\left[\frac{n_f P a y_{eff}}{2I_{eff}}\omega e^{-\omega x} + \frac{n_f P y_{eff}}{2I_{eff}}\right] \tag{11}$$

$$\tau = \frac{t_f}{2}\left[\frac{n_f P y_{eff}}{I_{eff}} + \frac{n_f P y_{eff} a}{I_{eff}}\omega e^{-\omega x}\right] \tag{12}$$

$$\omega^2 = \frac{2G_a}{t_a t_f E_f} \tag{13}$$

where x is the distance from the critical end of the CFRP strip; t_f is the thickness of the CFRP strip; P is the concentrated load; y_{eff} is the distance from the strip centroid to the neutral axis of the section; I_{eff} is the effective second moment of area and can be calculated using Eq. 14; e is the base of natural algorithm; G_a is the shear modulus of the adhesive; t_a is the thickness of the adhesive layer; and a is the distance from the critical end of the NSM strip to the nearest support.

$$I_{eff} = \left(\frac{M_{cr}}{M_a}\right)^3 I_g + \left(1 - \left(\frac{M_{cr}}{M_a}\right)^3\right)I_{cr} \tag{14}$$

where M_{cr} and M_{cr} are the cracking and the applied moments on a beam section, respectively; I_g is the transformed gross second moment of area in terms of concrete of the

strengthened section; and I_{cr} is the transformed second moment of area in terms of concrete of the cracked section.

Obviously, the interfacial shear stresses calculated using Eqs. 11 and 12 achieve the largest values when x is equal to zero (i.e. at the end of the FRP strip). By using the Mohr-Coulomb failure criterion, the interfacial shear stress at interfacial debonding failure of the FRP strip end, τ_{max}, can be determined from the following equation:

$$\tau_{max} = \frac{f_c f_t}{f_c + f_t} \tag{15}$$

where f_c is the concrete cylinder compressive strength; and f_t is the concrete tensile strength. Substituting Eq. 15 into Eq. 11 or Eq.12 with $x{=}0$ yields the applied load at interfacial debonding failure of the FRP strip end.

2.4 Summary

As can be seen from the above review, in the end cover separation strength model proposed by Al-Mahmoud et al. [22] and the end interfacial debonding strength model proposed by Hassan and Rizkalla [25], the concrete is assumed to be a linear elastic material in compression; in De Lorenzis and Nanni's model [21], the concept of effective length of the NSM FRP is introduced, and in the effective length region, the interfacial stress is assumed to be uniformly distributed. In all three models, the bonded interface between FRP and concrete and that between steel bars and concrete are assumed to experience no interfacial slips. Despite these assumptions, which may lead to significant prediction errors, they represent valuable attempts at formulating strength models for end debonding failures in RC beams strengthened with NSM FRP reinforcement.

9

In the present study, only Al-Mahmoud et al.'s model [22] and Hassan and Rizkalla's model [25] are compared with the present model. De Lorenzis and Nanni's model [21] was developed for NSM FRP round bars and cannot be easily adapted for use of NSM FRP strips. Although Al-Mahmoud et al.'s model [22] was originally proposed for RC beams strengthened with NSM round FRP bars, it can be easily modified for application to RC beams strengthened with NSM FRP strips: by replacing the formula for cross-sectional area for a circular section with that for a rectangular section.

When comparing Hassan and Rizkalla's model [25] with the present model in predicting end cover separation failure, it should be noted that the former is for end interfacial debonding while the latter is for end cover separation. However, it can be expected that the failure load predicted by Hassan and Rizkalla's model [25] should not be smaller than the test result as well as the prediction from the present model; otherwise, the beam should have failed by end interfacial debonding instead of end cover separation. The comparison thus can be used to check whether Hassan and Rizkalla's model [25] does provide an upper bound prediction.

3   SIMPLIFIED FE APPROACH FOR END COVER SEPARATION

The simplified FE model developed by Zhang and Teng [23, 24] for cover separation failure in FRP-strengthened RC beams was employed in a parametric study to generate numerical data for use in the formulation of a strength model. A brief summary of this simplified FE model is given herein to set the background for the parametric study. For more details of this simplified FE model, the reader is referred to Ref. [24].

In the simplified FE model, the segment of the RC beam between the two major cracks near the critical end of the FRP reinforcement is isolated to form the model for analysis (Fig. 3),

with the moments acting on the two cracked sections being imposed using two pairs of external loads (R and P_3 as one pair on the critical, left cracked section, and P_1 and P_2 as another pair on the other cracked section at the FRP strip end in Fig. 3). A rigid plate is attached to each cracked section to enforce the plane section assumption. As can be seen from Fig. 3, if the strain in the FRP reinforcement at the critical crack (Point B in Fig. 3) at end cover separation is known, the moment acting on the same section can be obtained through section analysis. The concrete is modelled using 4-node plane stress elements; the steel reinforcement is simulated using 2-node beams elements and both sides of the steel reinforcement are connected to the rigid plates. The cohesive-element-pair (CEP) proposed by Zhang and Teng [23, 24] is used to simulate the radial stresses exerted by the tension steel bars onto the surrounding concrete when they are in tension. The FRP is modelled using 2-node beam elements located at the centroid of the NSM FRP reinforcement. Only one end (the left end in Fig. 3) of the FRP reinforcement is connected to the adjacent rigid plate, while the other end (the right end) representing the actual end of the FRP reinforcement and is left free.

The behaviour of cracked concrete is simulated using the orthogonal fixed smeared crack model. The crack band concept [28] is employed in the simplified FE model with the fracture energy being that given by CEB-FIP [29]. The maximum tensile stress criterion is adopted to describe the initiation of cracking while the yield surface proposed by Buyukozturk [30] with the associated flow rule is used to describe the compression-dominated behaviour of concrete. The tension-softening behaviour and the shear stress-slip behaviour of cracked concrete as well as the compressive behaviour of concrete are properly modelled. The FRP is modelled as an elastic isotropic brittle material, and the steel reinforcement including tension bars, compression bars and stirrups is modelled as an elastic-perfectly plastic material. The

11

interfacial behaviour between longitudinal steel bars and concrete is simulated using the bond-slip model given in CEB-FIP 29] while that between NSM FRP strips and concrete is simulated using the bond-slip model proposed by Zhang et al. [31]. The latter means that the FE model is only applicable to RC beams strengthened in flexure with NSM CFRP strips although applicability to other forms of FRP reinforcement can be easily enabled by replacing Zhang et al.'s bond-slip model [31] with an appropriate model.

4   STRENGTH MODEL FOR END COVER SEPARATION

As explained earlier, if the strain in the FRP reinforcement at the critical cracked section (Point B in Fig. 3) at end cover separation failure (i.e. the debonding strain in the FRP or simply the debonding strain) can be obtained, a section analysis can be conducted to find the moment acting on the critical cracked section based on the plane section assumption, and the shear force and the load level of the beam can be easily found from the bending moment value for a given load distribution. The proposed debonding strength model for end cover separation failure thus consists of a method for predicting debonding strain and a conventional section analysis based on the plane section assumption, with the former being the key element. In the present study, the section analysis is based on the BS 8110 [32] compressive stress-strain curve of concrete, so the ultimate concrete compressive strain is taken to be 0.0035.

4.1 Debonding strain in the FRP at end cover separation

The FE approach described earlier was used to conduct a parametric study to generate numerical results for the development of an approximate analytical equation for the debonding strain. The following geometric and material properties define the reference case for the parametric study unless otherwise specified: concrete cylinder compressive strength

f_c =30 *MPa*; elastic modulus of FRP E_f =150 *GPa*; A_f = 40 *mm²*; thickness of FRP strip = 2 *mm*; second moment of area of FRP strip I_f = 1333 *mm⁴*; vertical distance between the centroids of the steel and the FRP reinforcements c_d = 30 *mm*; crack spacing s_c = 100 *mm* (length of the beam segment in the FE model); height of the beam h = 300 *mm*; width of the beam b = 150 *mm*; sum of diameters of all steel tensions bars D_t = 24 *mm* (i.e. $2\phi12$); and moment ratio between the right and the left cracked sections β_P =0.5.

4.2.1   *Effect of second moment of area of FRP strip*

The second moment of area of the FRP strip, I_f, was varied from $1\times10^3\ mm^4$ to $2\times10^4\ mm^4$ to examine its effect on the debonding strain. The cross-sectional area of the FRP strip was kept constant at 40 mm^2, but the height and thickness of the FRP strip cross-section were changed to achieve the desired I_f value. Note that for the reference beam with a width of 150 mm, $I_f = 5\times10^3\ mm^4$, which is a practically likely value (e.g. $I_f = 5.2\times10^3\ mm^4$ for two 2×25 mm NSM CFRP strips). Therefore, the selected range of I_f values was large enough to cover practical situations and to examine its influence.

The predicted debonding strains are listed in Table 1. The maximum difference between the predicted FRP strains is only about 2% within the range of I_f values investigated, so it may be concluded that for practical applications, the effect of I_f is minimal and can be neglected.

4.2.2   *Effect of beam height*

Table 2 provides the predicted debonding strains for three beam heights: h = 300 *mm*, 600

mm, and 900 *mm*; all other properties are the same as those of the reference case. Clearly the effect of beam height is also insignificant, so it can also be neglected in evaluating the debonding strain in the FRP.

4.2.3   *Effect of moment ratio*

The effect of moment ratio β_P was examined for three different concrete strengths ($f_c = 20$ *MPa*, 30 *MPa* and 40 *MPa*), four values of the distance between the steel and the FRP reinforcements ($c_d = 15$ *mm*, 30 *mm*, 45 *mm*, and 60 *mm*), and four different crack spacings ($s_c = 50$ *mm*, 75 *mm*, 100 *mm*, and 150 *mm*). In each case, the moment ratio between the right and the left cracked sections was varied from 0 to 1.0 at an interval of 0.1. The predicted debonding strains, normalized with respect to the debonding strain of the corresponding case with a moment ratio of 0.6, are shown in Fig. 4. For ease of reference, each numerical case (or numerical specimen) in Fig. 4 is given a name, which starts with a number to represent the cylinder compressive strength of concrete (f_c), followed by a number to represent the elastic modulus of FRP (E_f), and then a number to represent the distance between steel and FRP reinforcements (c_d), and finally a number to represent the crack spacing (s_c). It is seen that as the moment ratio increases, the debonding strain first increases nearly linearly regardless of the values of the other parameters (i.e. f_c , c_d and s_c) until the moment ratio reaches 0.6; afterwards, the debonding strain decreases nearly linearly. All of the normalized curves shown in Fig. 4 are almost identical to each other, with most values falling in the range from 0.9 to 1. The effect of moment ratio on the debonding strain is therefore small and is ignored in the approximate predictive equation for debonding strain presented later in the paper.

4.2.4 Effect of axial rigidity of FRP strip

The axial rigidity of the FRP strip $A_f E_f$ was varied from 2000 kN ($20\,mm^2 \times 100\,GPa$) to 16000 kN ($80\,mm^2 \times 200\,GPa$) to study its effect on the debonding strain. The relationship between the FRP debonding strain obtained from FE analysis and the reciprocal of FRP axial rigidity $A_f E_f$ is plotted in Fig. 5, from which it can be seen that the variation of the FE debonding strain with the reciprocal of FRP strip axial rigidity follows approximately a power function.

4.2.5 Effect of concrete strength

The effect of concrete strength f_c was examined for three different values of the elastic modulus of FRP (E_f = 100 GPa, 150 GPa, and 200 GPa) and four different values of the cross-sectional area of FRP strip (A_f = 20 mm^2, 40 mm^2, 60 mm^2 and 80 mm^2). The other geometric and material properties of the beams were the same as those of the reference beam. The predicted relationship between the debonding strain and the concrete strength is shown in Fig. 6, which indicates that the FRP strain is approximately proportional to $\sqrt{f_c}$. Each numerical specimen in Fig. 6 is given a name, which starts with a number to represent the elastic modulus of FRP (E_f) and is then followed by a number to represent the cross-sectional area of FRP strip (A_f).

4.2.6 Effects of crack spacing and distance between steel and FRP reinforcements

The effect of distance between steel reinforcement and FRP reinforcements, c_d, was examined by obtaining FE predictions for four different values: 15 mm, 30 mm, 45 mm, and 60 mm. The effect of crack spacing, s_c, was also examined by obtaining FE predictions for

four different values: 50 *mm*, 75 *mm*, 100 *mm*, and 150 *mm*. The relationship between the debonding strain and c_d is shown in Fig. 7 while that between the debonding strain and s_c is shown in Fig. 8. Fig. 7 indicates that the debonding strain decreases nearly linearly as the value of c_d increases, with the slopes of the linear best-fit lines for different s_c values being nearly the same. Fig. 8 indicates that the debonding strain increases with the value of s_c. As the value of c_d increases, the relationship between the debonding strain and s_c changes from a power function to a linear function. To see a clearer trend, the debonding strains normalized with respect to the strain of the case with a c_d value of 30 mm are shown in Fig. 9, which indicates that the normalized strain decreases nearly linearly as the value of c_d increases regardless of the values of s_c and the magnitude of slope of the linear best-fit lines decreases as the value of s_c increases.

4.2.7   *Effects of beam width and sum of steel tension bar diameters*

The debonding strain in the FRP is expected to be proportional to the clear width of the beam $b_{\text{clear}} = b - D_t$, where D_t is the sum of all steel tension bar diameters, if other parameters are the same. Furthermore, the debonding strain is expected to depend on the b_{clear}/D_t ratio as the effect of radial stresses from steel tension bars is affected by the b_{clear}/D_t ratio. In the parametric study, the following beam widths were examined: 50 *mm*, 100 *mm*, 150 *mm*, 200 *mm*, and 250 *mm*, with the corresponding b_{clear}/D_t ratios being 1.08, 3.17, 5.25, 7.33 and 9.42. The corresponding values chosen for the cross-sectional area of the FRP strip, A_f, are 8.25 *mm*^{2}, 24.13 *mm*^{2}, 40.00 *mm*^{2}, 55.88 *mm*^{2} and 71.75 *mm*^{2}, in order to keep the A_f/b_{clear}

ratio constant. Fig. 10 shows that the predicted debonding strain increases with the b_{clear}/D_t ratio approximately following a power function.

4.2.8 Approximate equation for the debonding strain

Based on the regression analysis of the results of 168 numerical specimens examined in the parametric study, Eq. 16 is proposed as a design model for predicting the debonding strain in the FRP at end cover separation failure:

$$\varepsilon_{db} = 10^4 \times \beta_{cs}\beta_{AE}\beta_{bod}b_{clear}\sqrt{f_c} \tag{16}$$

$$\beta_{cs} = (\frac{4.5}{s_c^{0.3}} - \frac{c}{s_c})(\frac{s_c}{100} - 0.1) \tag{17}$$

$$\beta_{AE} = \frac{1}{\left(A_f E_f\right)^{0.9}} \tag{18}$$

$$\beta_{bod} = \left(\frac{b_{clear}}{D_t}\right)^{0.1} \tag{19}$$

where β_{cs} reflects the combined effect of c_d (distance between the steel and the FRP reinforcements, in *mm*) and s_c (crack spacing, in *mm*); β_{AE} reflects the effect of axial rigidity of FRP strip $A_f E_f$ (A_f in *mm²* and E_f in *GPa*); and β_{bod} reflects the effect of ratio between beam clear width b_{clear} (in *mm*) and sum of steel tension bar diameters D_t (in *mm*). The concrete cylinder strength f_c is in *MPa*.

A comparison between the predictions of the simplified FE model and the analytical debonding strain equation (Eq. 16) is shown in Fig. 11, indicating very close agreement between the two sets of results. The ratios between the analytical and the FE predictions have an average value of 1.00, a standard deviation (STD) of 0.070 and a coefficient of variation

17

(CoV) of 0.070.

4.2 Crack spacing

To determine the debonding strain as well as the distance between the left cracked section and the nearest support, the crack spacing is needed as input. In the present study, the minimum stabilized crack spacing, $s_c^{\min}$, proposed by Zhang et al. [26] is adopted:

$$s_c^{\min} = \frac{A_e f_t}{u_s \sum O_{bars} + u_f C_{failure}}$$

(21)

where $u_f = 0.28\sqrt{f_{cu}}$ is the average shear bond strength between FRP and concrete, $C_{failure}$ is the perimeter length of the failure plane which is taken to be the total length of the three groove sides. In the next section, the minimum stabilized crack spacing, $s_c^{\min}$, the maximum stabilized crack spacing, $2s_c^{\min}$, and an intermediate value, $1.5s_c^{\min}$, are all examined to investigate the effect of crack spacing.

5 COMPARISON WITH TEST DATA

For the proposed debonding strain equation for end cover separation to be used with confidence in practical design, its accuracy needs to be assessed using laboratory test data. The test data of 10 RC beams strengthened with NSM FRP strips were collected from the published literature for this purpose. For all these 10 beams, sufficient details have been provided in the papers for them to be used in the comparison. Details of these 10 test beams are given in Tables 3 and 4. In addition to the present debonding strength model, the models of Al-Mahmoud et al. [22] and Hassan and Rizkalla [25] are also included in the comparison.

The predictions of the present debonding strength model for three different crack spacings

(i.e. $s_c = s_c^{min}$, $1.5 s_c^{min}$ and $2 s_c^{min}$ respectively) are compared in Fig. 12 with the test results. The predictions of the two existing models for these 10 RC beams are compared with the test results in Figs. 13 and 14 respectively. All the analytical predictions and the test results for the shear force are listed in Tables 5.

The proposed strength model with a crack spacing of $1.5 s_c^{min}$ leads to an average prediction-to-test ratio of 1.10, a STD of 0.119 and a CoV of 0.108 (Table 5). These statistical indicators are better than those for predictions of the proposed strength model obtained with crack spacings of s_c^{min} and $2 s_c^{min}$, for which the average prediction-to-test ratios are 0.863 and 1.17, the STDs are 0.155 and 0.172, and the CoVs are 0.180, 0.147 respectively. Nevertheless, the proposed strength model with any of the three crack spacing values offers much closer predictions of the test results than the two existing models proposed by Al-Mahmoud et al. [22] and Hassan and Rizkalla [25] respectively. The predictions from Hassan and Rizkalla's model [25] are very conservative with a large scatter, with the prediction-to-test average ratio, STD and CoV being 0.555, 0.259 and 0.467 respectively, indicating that Hassan and Rizkalla's model [25] fails to provide a reasonable upper bound prediction. The predictions of Al-Mahmoud et al.'s model [22], on the contrary, are very un-conservative with an even larger scatter, with the average prediction-to-test ratio, STD and CoV being 1.90, 1.34 and 0.702 respectively. The superior performance of the proposed debonding strength model is also clearly demonstrated by the comparisons given in Figs. 12 to 14.

7   CONCLUDING REMARKS

This paper has been concerned with the development of an analytical model for predicting the end cover separation failure load of RC beams strengthened with FRP strips (i.e. rectangular

FRP bars with a sectional height-to-thickness ratio not less than 5). The approach taken was to develop an analytical equation for the debonding strain in the FRP strips at the critical cracked section at end cover separation failure (i.e. the debonding strain) and to find the moment acting in the critical cracked section by conventional section analysis based on the plane section assumption (i.e. the debonding moment). Once the debonding moment is known, the associated shear force and the load level at cover separation failure can be easily determined for any given load distribution. The analytical equation for the debonding strain is thus the key element of the proposed debonding strength model. In practice, the alternative approach of checking the strain in the FRP strips at the critical cracked section against the prediction of the proposed debonding strain equation can be adopted to design again cover separation failure.

To formulate an analytical equation for the debonding strain, an efficient FE approach recently proposed by the authors [23, 24] was employed in a parametric study to obtain extensive numerical results. These results were presented and examined to understand how each parameter affects this debonding strain, based on which an appropriate analytical equation for the debonding strain was proposed. The proposed strength model as well as with two existing strength models for end debonding failure was compared with a test database assembled from the published literature. These comparisons showed that the proposed strength model leads to predictions in close agreement with the test results and is far more accurate than the two existing models.

8   ACKNOWLEDGEMENT

9 REFERENCES

[1]   Teng, J. G., Chen, J. F., Smith, S. T., and Lam, L. (2002). *FRP-strengthened RC Structures*, West Sussex: Wiley.

[2]   Oehlers, D. J. and Seracino, R. (2004). *Design of FRP and steel plated RC structures: retrofitting beams and slabs for strength, stiffness and ductility*. Elsevier.

[3]   Bank L.C. (2006). *Composites for construction: Structural design with FRP materials*. West Sussex: Wiley, UK.

[4]   Hollaway, L. C. and Teng, J. G., eds. (2008). *Strengthening and rehabilitation of civil infrastructures using FRP composites*, Woodhead, Cambridge, U.K.

[5]   Barros, J. A. O., Dias, S. J. E., and Lima, J. L. T. (2007). "Efficacy of CFRP-based techniques for the flexural and shear strengthening of concrete beams." *Cement & Concrete Composites*, 29(3), 203-217.

[6]   De Lorenzis, L. and Teng, J. G. (2007). "Near-surface mounted FRP reinforcement: an emerging technique for strengthening structures." *Composites: Part B*, 38(2), 119-143.

[7]   Soliman, S.M., El-Salakawy, E. and Benmokrane, B. (2011). "Bond performance of near-surface-mounted FRP bars." *Journal of Composites for Construction, ASCE*, 15(1), 103-111.

[8]   Zhang, S. S. (2012). *Behaviour and modelling of RC beams strengthened in flexure with near-surface mounted FRP strips*. PhD thesis, The Hong Kong Polytechnic University, Hong Kong, China.

[9]   El Hacha, R. and Rizkalla, S.H. (2004). "Near-surface-mounted fiber-reinforced polymer reinforcements for flexural strengthening of concrete structures." *ACI*

Structural Journal, 101(5), 717-726.

[10] Perera, W.K.K.G., Ibell, T.J. and Darby, A. P. (2009). "Bond behaviour and effectiveness of various shapes of NSM CFRP bars." *Proceedings, 9th International Symposium on Fiber-Reinforced Polymers Reinforcement for Concrete Structures (FRPRCS-9)*, 13-15 July, Sydney, Australia (CD-ROM).

[11] Zhang, S. S., Teng, J. G. and Yu, T. (2014). "Bond strength model for CFRP strips near-surface mounted to concrete." *Journal of Composites for Construction*, *ASCE*, 18, SPECIAL ISSUE: 10th Anniversary of IIFC, A4014003.

[12] Zhang, S.S. and Teng, J.G. (2014). "Finite element analysis of end cover separation in RC beams strengthened in flexure with FRP", *Engineering Structures*, 75, 550-560.

[13] Arduini, M., Tommaso, A. D., and Nanni, A. (1997). "Brittle failure in FRP plate and sheet bonded beams." *ACI Structural Journal* 94(4), 363-370.

[14] Rahimi, H. and Hutchinson, A. (2001). "Concrete beams strengthened with externally bonded FRP plates." *Journal of Composites for Construction, ASCE*, 5(1), 44-56.

[15] Pham, H.B. and Al-Mahaidi, R. (2005) "Finite element modelling of RC beams retrofitted with CFRP fabrics." *Proceedings, 7th International Symposium on Fiber Reinforced Polymer Reinforcement for Reinforced Concrete Structures*, American Concrete Institute 2005, SP-230, 499-514.

[16] Oehlers, D. J. (1992). "Reinforced-concrete beams with plates glued to their soffits." *Journal of Structural Engineering, ASCE*, 118(8), 2023-2038.

[17] Oehlers, D. J., Liu, I. S. T., Seracino, R. and Ali, M. S. M. (2004). "Prestress model for shear deformation debonding of FRP- and steel-plated RC beams." *Magazine of Concrete Research*, 56(8), 475-486.

[18] Gao, B., Leung, C. K. Y. and Kim, J. K. (2005). "Prediction of concrete cover separation failure for RC beams strengthened with CFRP strips." *Engineering*

Structures, 27(2), 177-189.

[19] Teng, J. G. and Yao, J. (2007). "Plate end debonding in FRP-plated RC beams-II: strength model." *Engineering Structures*, 29(10), 2472-2486.

[20] Zhang, S. S. and Teng, J. G. (2010). "Finite element prediction of plate-end cover separation in FRP-strengthened RC beams." *Proceedings, 11th International Symposium on Structural Engineering*, December 18-20, 2010, Guangzhou, China, pp. 1794-1799.

[21] De Lorenzis, L. and Nanni, A. (2003). "Proposed design procedure of NSM FRP reinforcement for strengthening of RC beams." *Proceedings, 6th International Symposium on FRP Reinforcement for Concrete Structures*, July 8-10, 2003, Singapore, pp. 1455-1464.

[22] Al-Mahmoud, F., Castel, A., Francois, R., and Tourneur, C. (2010). "RC beams strengthened with NSM CFRP rods and modeling of peeling-off failure." *Composite Structures*, 92(8), 1920-1930.

[23] Zhang, S.S. and Teng, J.G. (2013). "Simplified finite element modelling of end cover separation in RC beams flexurally-strengthened with bonded FRP reinforcement." *Proceedings, 4th Asia Pacific Conference on FRP Composites in Structures (APFIS)*, December, 11-13, 2013, Melbourne, Australia. (CD-ROM).

[24] Zhang, S.S. and Teng, J.G. (2015). "End cover separation in RC beams strengthened in flexure with bonded FRP reinforcement: simplified finite element approach." Materials and Structures, accepted for publication.

[25] Hassan, T. K. and Rizkalla, S. H. (2003). "Investigation of bond in concrete structures strengthened with near surface mounted carbon fiber reinforced polymer strips." *Journal of Composites for Construction, ASCE*, 7(3), 248-257.

[26] Zhang, S., Raoof, M. and Wood, L. A. (1995). "Prediction of peeling failure of

reinforced-concrete beams with externally bonded steel plates." *Proceedings, the Institution of Civil Engineers-Structures and Buildings*, 110(3), 257-268.

[27] Malek, A. M., Saadatmanesh, H. and Ehsani, M. R. (1998). "Prediction of failure load of R/C beams strengthened with FRP plate due to stress concentration at the plate end." *ACI Structural Journal*, 95(1), 142-152.

[28] Bazant, Z.P. and Oh, B.H. (1983). "Crack band theory for fracture of concrete." *Materials and Structures*, 16(93), 155-177.

[29] CEB-FIP. (1993). *Model Code 90*, Lausanne, Switzerland.

[30] Buyukozturk, O. (1997). "Nonlinear analysis of reinforced concrete structures." *Computers and Structures* , 7, 149-156.

[31] Zhang, S.S., Teng, J.G. and Yu, T. (2013). "Bond-slip model for CFRP strips near-surface mounted to concrete." *Engineering Structures*, 56, 945–953.

[32] BS 8110. (1997). *Structural use of concrete-part 1: Code of practice for design and construction*, London: British Standards Institute, UK.

[33] Barros, J. A. O. and Fortes, A. S. (2005). "Flexural strengthening of concrete beams with CFRP laminates bonded into slits." *Cement & Concrete Composites*, 27(4), 471-480.

[34] Teng, J. G., De Lorenzis, L., Wang, B., Rong, L., Wong, T. N. and Lam, L. (2006). "Debonding failures of RC beams strengthened with near-surface mounted CFRP strips." *Journal of Composites for Construction, ASCE*, 10(2), 92-105.

[35] Thorenfeldt, E. (2007). "Bond capacity of CFRP strips glued to concrete in sawn slits." *Proceedings, 8th International Conference on Fibre Reinforced Plastics for Reinforced Concrete Structures*, July 16-18, 2007, Patras, Greece (CD-ROM).

10 TABLES

Table 1. Effect of second moment of area of FRP bar on debonding strain

Second moment of area of FRP bar I_f (mm^4)	Debonding strain ε_{db} ($\mu\varepsilon$)	Percentage reduction
1×10^3	2483	0.00%
5×10^3	2472	0.44%
1×10^4	2455	1.13%
2×10^4	2435	1.93%

Table 2. Effect of beam height on debonding strain

Beam height h (mm)	Debonding strain ε_{db} ($\mu\varepsilon$)	Percentage reduction
300	2482	0.00%
600	2453	1.17%
900	2416	2.66%

Table 3. Details of RC beams strengthened with NSM FRP

Source	Specimen	b (mm)	h (mm)	h_0 (mm)	a (mm)	a_v (mm)	L (mm)	f_c (MPa)	E_c (GPa)
Ref. [33]	V2R2	100	177	157	50	500	1500	46.1	32.1
	V3R2	100	175	155	50	500	1500	46.1	32.1
	V4R3	100	180	160	50	500	1500	46.1	32.1
Ref. [34]	B500	150	300	256	1200	1200	3000	35.2	28.1
	B1200	150	300	256	900	1200	3000	35.2	28.1
	B1800	150	300	256	600	1200	3000	35.2	28.1
Ref. [5]	S2	120	170	146	60	300	900	52.2	34.2
	S3	120	170	146	60	300	900	52.2	34.2
Ref. [35]	B2	150	250	206	100	950	2500	50.0	33.4
	B5	150	250	206	100	950	2500	50.0	33.4

Note: b = width of beam; h = height of beam; h_0 = effective depth of beam; a = distance from a bar end to the nearest support; a_v = shear span of beam; L = span of beam; f_c = cylinder compressive strength of concrete; and E_c = elastic modulus of concrete.

Table 4. Details of steel bars and FRP strips for the test beams

Source	Specimen	E_f (GPa)	f_f (MPa)	t_f (mm)	h_f (mm)	E_s^{ten} (GPa)	f_y^{ten} (GPa)	A_s^{ten} (mm²)	$(n/\phi)_{ten}$	E_s^{com} (GPa)	f_y^{com} (GPa)	A_s^{com} (mm²)	$(n/\phi)_{com}$	E_{vc} (GPa)	f_{vy} (GPa)	A_{vc} (mm²)	s_v (mm)
Ref. [33]	V2R2	158.8	2739.5	2.9	9.59	200	730	84.8	3/6	200	730	101	2/8	200	730	56.5	100
	V3R2	158.8	2739.5	2.9	9.59	200	730	107	2/6+1/8	200	730	101	2/8	200	730	56.5	100
	V4R3	158.8	2739.5	4.35	9.59	200	730	151	3/6	200	730	101	2/8	200	730	56.5	100
Ref. [34]	B500	151	2068	4	16	210	532	226	2/12	210	375	101	2/8	210	375	101	100
	B1200	151	2068	4	16.	210	532	226	2/12	210	375	101	2/8	210	375	101	100
	B1800	151	2068	4	16	210	532	226	2/12	210	375	101	2/8	210	375	101	100
Ref. [5]	S2	158.8	2740	2.8	9.6	200	627	66.4	2/6.5	200	627	66.4	2/6.5	200	540	56.5	80
	S3	158.8	2740	4.2	9.6	200	627	99.5	3/6.5	200	627	66.4	2/6.5	200	540	56.5	80
Ref. [35]	B2	157	2580	6	15	203	530	226	2/12	203	530	226	2/12	200	530	101	100
	B5	153	2500	5	20	203	530	226	2/12	203	530	226	2/12	200	530	101	100

Note: E_f = elastic modulus of FRP; f_f = tensile strength of FRP; t_f = thickness of FRP strip; h_f = height of FRP strip; E_s^{ten} = elastic modulus of steel tension bars; f_y^{ten} = yield stress of steel tension bars; A_s^{ten} = total cross-sectional area of steel tension bars; $(n/\phi)_{ten}$ = number/diameter of tension steel bars; E_s^{com} = elastic modulus of steel compression bars; f_y^{com} = yield stress of steel compression bars; A_s^{com} = total cross-sectional area of steel compression bars; $(n/\phi)_{com}$ = number/diameter of steel compression bars; E_{vc} = elastic modulus of stirrups; f_{vy} = yield stress of stirrups; A_{vc} = total cross-sectional area of stirrups; s_v = spacing of stirrups.

Table 5. Test and predicted ultimate shear forces for beams strengthened with NSM FRP

Source	Specimens	V_{test} (kN)	$V_{pre,1}$ (kN)	$\dfrac{V_{pre,1}}{V_{test}}$	$V_{pre,1.5}$ (kN)	$\dfrac{V_{pre,1.5}}{V_{test}}$	$V_{pre,2}$ (kN)	$\dfrac{V_{pre,2}}{V_{test}}$	V_{H-R} (kN)	$\dfrac{V_{H-R}}{V_{test}}$	V_{AI} (kN)	$\dfrac{V_{AI}}{V_{test}}$
Ref. [33]	V2R2	39.25	40.7	1.04	50.3	1.28	55.3	1.41	34.7	0.884	143	3.64
	V3R2	40.95	43.2	1.05	54.4	1.33	60.4	1.48	36.2	0.885	166	4.04
	V4R3	47.45	36.1	0.761	49.5	1.04	57.5	1.21	33.6	0.708	160	3.35
Ref. [34]	B500	23.9	17.0	0.710	24.7	1.03	25.4	1.06	5.10	0.213	15.1	0.631
	B1200	31.55	21.9	0.694	31.4	0.995	32.0	1.01	6.70	0.214	19.6	0.622
	B1800	45.85	30.9	0.673	43.2	0.942	43.1	0.940	10.0	0.218	28.2	0.614
Ref. [5]	S2	46.65	52.2	1.12	49.7	1.07	45.5	0.976	30.3	0.649	97.2	2.08
	S3	48.3	42.3	0.877	51.4	1.07	56.0	1.16	27.8	0.576	94.1	1.95
Ref. [35]	B2	63.9	59.1	0.925	74.9	1.17	83.3	1.30	36.4	0.542	69.9	1.04
	B5	65.5	51.4	0.785	67.5	1.03	76.5	1.17	41.5	0.610	66.2	0.973
Statistical indicators	**Average =**			0.863		1.10		1.17		0.555		1.90
	STD =			0.155		0.119		0.172		0.259		1.34
	CoV =			0.180		0.108		0.147		0.467		0.702

Note: $V_{pre,1}$ = shear force predicted by the proposed model with s_c^{min} ;

$V_{pre,1.5}$ = shear force predicted by the proposed model with $1.5 s_c^{min}$;

$V_{pre,2}$ = shear force predicted by the proposed model with $2 s_c^{min}$;

V_{H-R} = shear force predicted by Hassan and Rizkalla's model [25]; and

V_{AI} = shear force predicted by Al-Mahmoud et al.'s model [22].

11 FIGURES
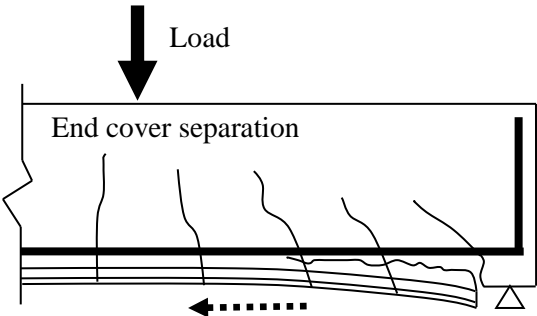
Fig. 1 Schematic of end cover separation
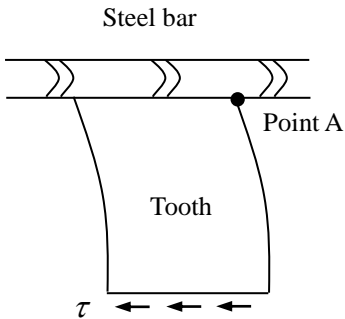
Fig. 2. Concrete tooth between two adjacent cracks
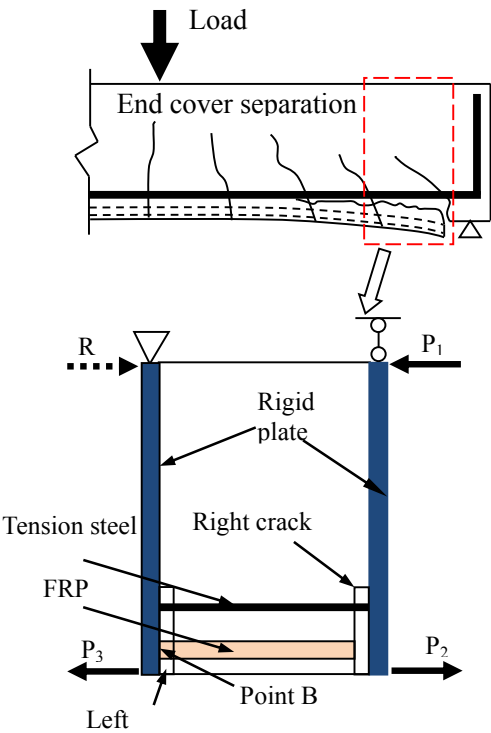
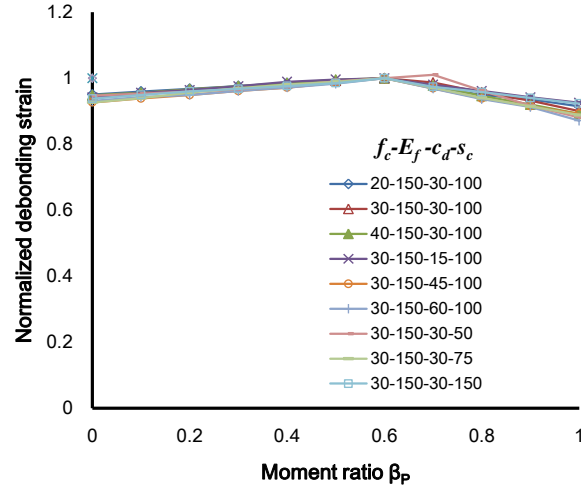Fig. 3. Simplified finite element model

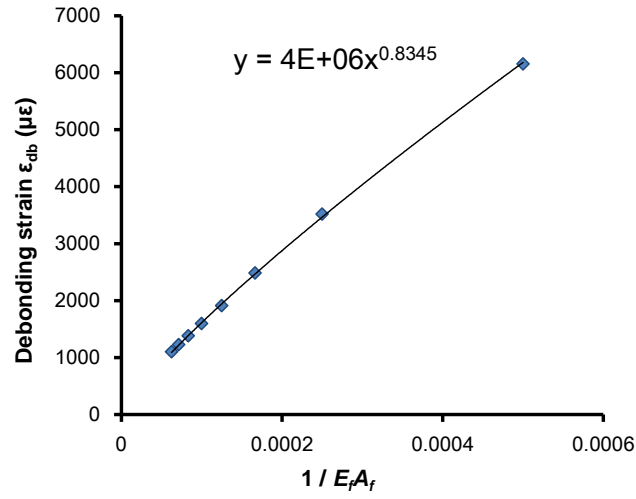Fig. 4. Effect of moment ratio on normalized debonding strain

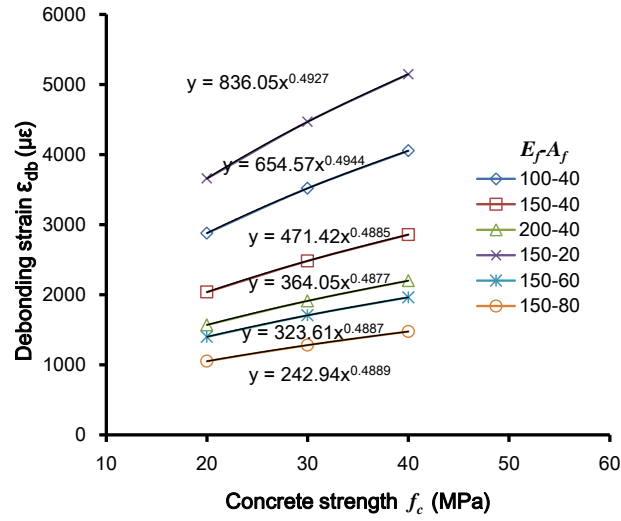Fig. 5. Effect of axial rigidity of FRP on debonding strain

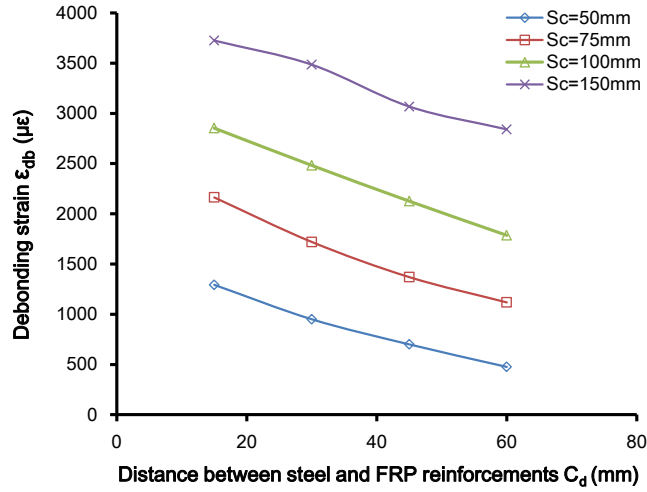Fig. 6. Effect of concrete strength on debonding strain

29

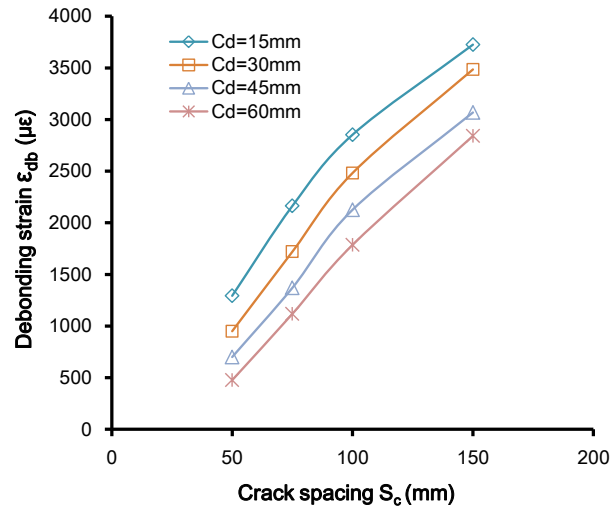Fig. 7. Effect of distance between steel and FRP reinforcements on debonding strain
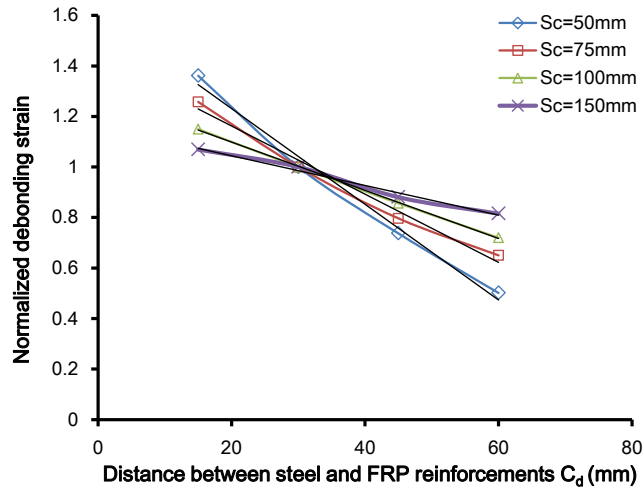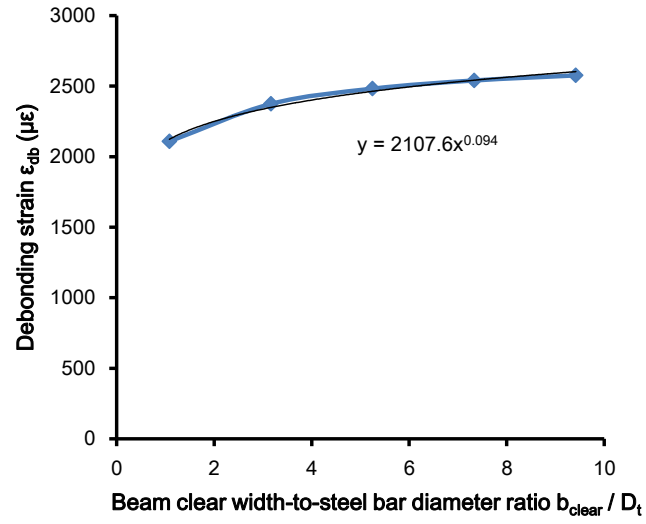

Fig. 8. Effect of crack spacing on debonding strain

Fig. 9. Effect of distance between steel and FRP reinforcements on normalized debonding strain

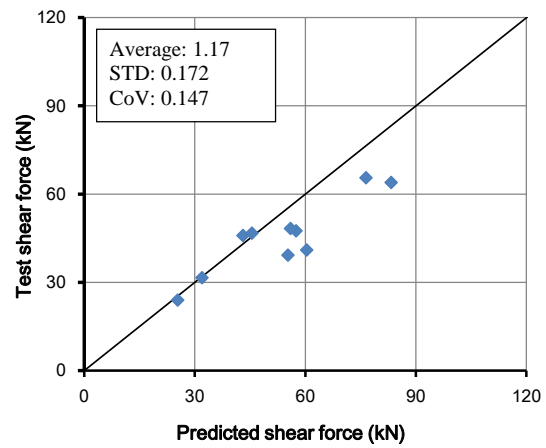Fig. 10. Influence of beam clear width-to-steel bar diameter ratio on debonding strain
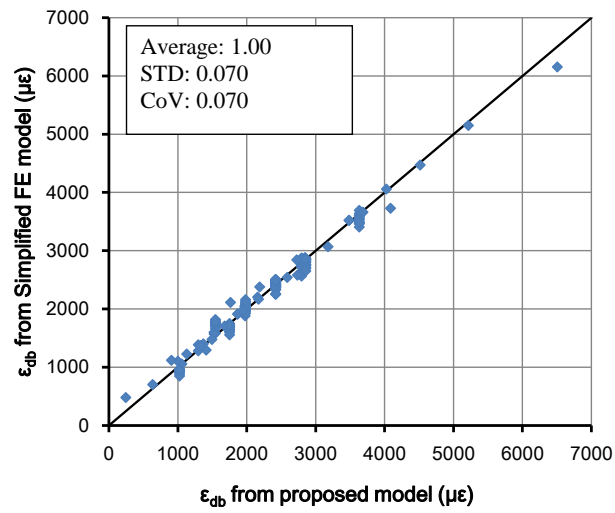
Fig. 11. Comparison of debonding strain between FE predictions and proposed strength model
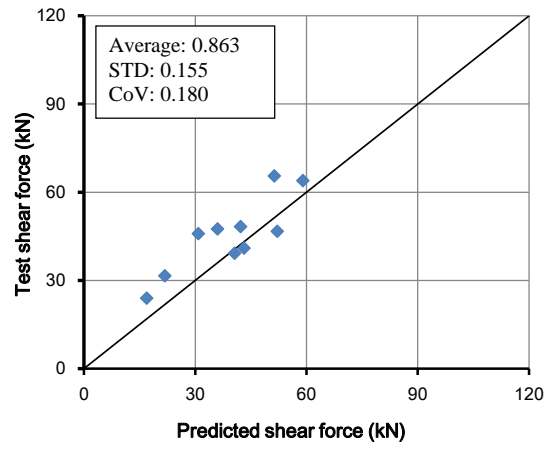
(a) Crack spacing $= s_c^{\min}$
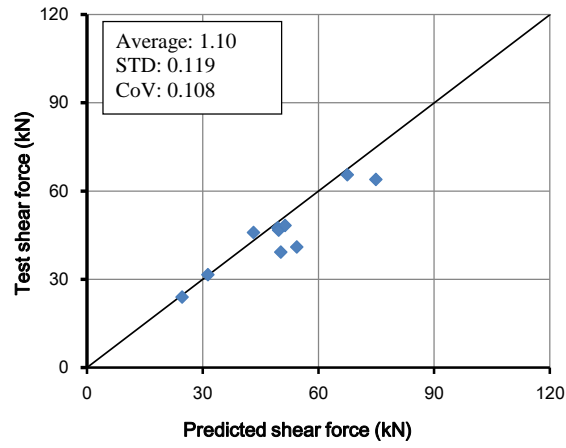
(b) Crack spacing $= 1.5 s_c^{\min}$

(c) Crack spacing $= 2 s_c^{\min}$

Fig. 12. Comparison of shear force at debonding between tests and proposed strength model
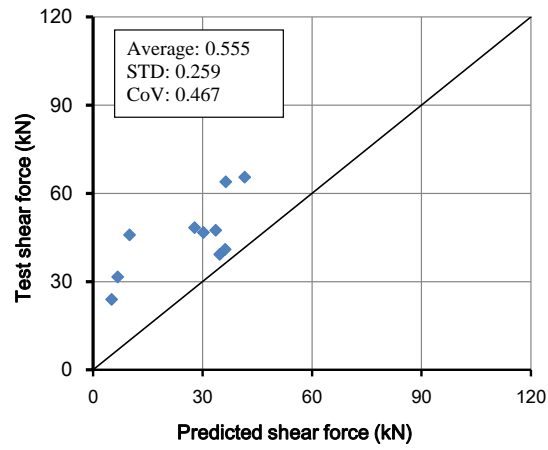
Fig. 13. Comparison of shear force at debonding between tests and Hassan and Rizkalla's model [25]
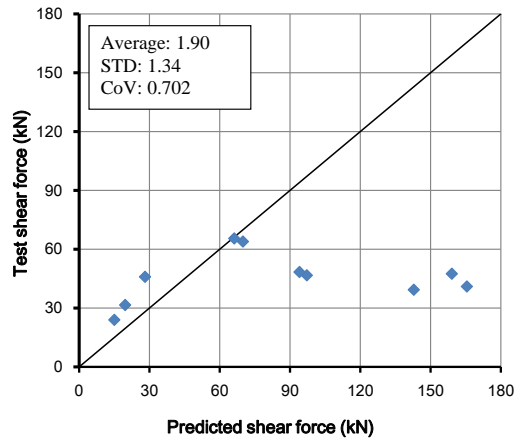

Fig. 14. Comparison of shear force at debonding between tests and Al-Mahmoud et al.'s model [22]